METHOD FOR CORRELATING NMR RELAXOMETRY AND MERCURY INJECTION DATA

D. Marschall, J. S. Gardner, D. Mardon, G. R. Coates (NUMAR Corp., Houston, TX)

ABSTRACT

We describe a methodology for correlating mercury injection capillary pressure (MICP) data with NMR transverse relaxation time (T_2) distributions to obtain estimates of immobile water saturation and permeability. Surface relaxivities determined from correlations computed for a suite of rock cores having diverse origins and properties are consistent with prior studies which show that carbonates generally have lower relaxivities than sandstones. A new, trial definition of immobile fluid volume based on fractional flow concepts is introduced and compared to existing interpretation models that use a fixed T_2 cutoff to distinguish mobile vs. immobile fluid. An NMR-based analog of the Swanson parameter is shown to be an excellent predictor of permeability whereas porosity is essentially uncorrelated with permeability.

INTRODUCTION

Water-cut prediction is perhaps the most common petrophysical application of nuclear magnetic resonance (NMR) logging data. The basic interpretation scheme involves a comparison between bulk volume water (BVW) computed from conventional porosity and resistivity log data and the irreducible fluid (BVI) and "free" fluid (FFI) volumes from NMR. For a zone exhibiting significant free-fluid volume, BVI<BVW indicates at least some water will be produced whereas BVI≅BVW indicates the zone should produce hydrocarbons at no water-cut.

The principle underlying the FFI vs. BVI interpretation is that the transverse (T_2) relaxation time distribution measured by NMR represents the rock pore size distribution. A cutoff value of T_2 is used to distinguish immobile fluid (BVI) in small pores from mobile fluid (FFI) in larger pores. This scheme is based on the fast-diffusion relationship, established for water-saturated rocks[1], between pore volume-to-surface ratio V/S and T_2 given by

$$T_2^{-1} = \rho\,(V/S) \qquad (1)$$

where ρ is the surface relaxivity. Thus, a constant relaxation time cutoff corresponds to a fixed pore size and, hence, a fixed capillary pressure. These models also assume that 1) the formation interval of interest is water-wet, 2) the cutoff T_2 has a known, constant value, and 3) the viscosity of the oil, if present, is low enough that the T_2 of the oil signal is larger than the FFI-BVI cutoff value.

The purpose of this paper is to illustrate two novel applications of NMR T_2 distribution data. One application develops an alternative estimator of immobile fluid volume based on fractional flow concepts. The other application shows how to estimate permeability using

an NMR-derived analog of Swanson's parameter. Examples are shown using mercury injection capillary pressure measurements together with laboratory NMR data for a suite of sandstone and carbonate core samples of diverse properties and origins.

SAMPLES AND EXPERIMENTAL METHODS

Table 1 lists the samples used in this study along with standard core analysis and basic NMR data for each sample. All the samples are 1-inch long by 1-inch diameter plugs cut from whole core retrieved from six different wells. There are 17 plug samples in all comprising 3 clean sandstones, 5 shaly sandstones, 7 limestones and 2 dolostones. Together, these samples cover wide ranges of porosity (6.4 to 27. p.u.) and permeability (0.078 to 4450 md).

Prior to making NMR measurements, each plug was cleaned by hot solvent extraction. Resaturation porosity, steady state air permeability, and grain density were measured on each sample by a single commercial laboratory. The samples were then vacuum-pressure saturated with an NaCl brine whose concentration was adjusted to approximate the connate water salinity of the formation of origin (range = 35 to 200 kppm).

The mercury injection capillary pressure (MICP) data used in this study are of two different types. All samples except those from Well #1 have high-pressure MICP data. Each high-pressure MICP curve consists of at least 100 pressure vs. injection volume measurements that are roughly logarithmically spaced between ≤1psi to ≥50 kpsi air/mercury pressure. Samples from Well #1, have low-pressure MICP data with 24 points per curve between ~1 and 2000 psi. For the purpose of comparing NMR and MICP data, mercury capillary pressure Pc (in psi) was converted to a pore radius r (in μm) using the standard (Washburn) equation, i.e.,

$$r = 0.29\,\sigma\cos\theta/Pc, \qquad (2)$$

with an interfacial tension σ = 480 dyne/cm and a contact angle θ = 140°.

Proton NMR measurements were made on all the samples at 100% brine saturation using a commercially available core analyzer operating at 32°C and approximately 1 MHz. T_2 measurements were made in a homogeneous magnetic field using the CPMG method with phase alternation and an interecho spacing TE=0.5 msec. A sufficient number of echo trains were measured and stacked to achieve a minimum signal-to-noise ratio of 200:1 (300:1 typ.). T_2 distributions were computed by fitting the stacked echo trains for partial porosity amplitudes corresponding to 51 pre-selected values of T_2 spaced logarithmically between 0.1 and 10,000 msec using the algorithm developed by Prammer[2].

CORRELATION OF NMR T_2 AND MERCURY INJECTION DISTRIBUTIONS

Figure 1 shows comparisons between NMR T_2 and MICP distributions for the clean sand and carbonate samples (6 through 17), all of which have high-pressure MICP data. Figure 2 shows the same comparison for shaly sand samples (1 through 6) having low-pressure

MICP data. In order to place all the distributions on a common scale, MICP pore radii were converted to an equivalent T_2 value according to

$$T_2 = \frac{1000\,r}{2\rho_e} \qquad (3)$$

where T_2 is in msec, mercury injection pore radius r is in μm, and ρ_e is the effective relaxivity in μm/sec. Equation 3 is obtained by substituting the surface-to-volume ratio for cylindrical tube, i.e., S/V = 2/r, into Equation 1. The effective relaxivity ρ_e is introduced in Equation 3 to account for the fact that NMR responds to pore "body" size whereas MICP is controlled by the sizes of pore "throats". Thus, ρ_e is proportional to the product of the intrinsic relaxivity ρ (Equation 1) and a pore throat-to-body size ratio.

An effective relaxivity ρ_e that scales mercury pore radius r into T_2 (Equation 3) was determined for each sample by finding a best match between its MICP and T_2 distributions. The distribution matching was done quantitatively using a slight modification of the procedure described by Kleinberg and others[3]. Briefly, the procedure involves finding the value of ρ_e that minimizes the cross-correlation function C given by

$$C(\rho_e) = \Sigma\, a_{NMR}(T_2)\cdot a_{MICP}(1000r/2\rho_e) \qquad (4)$$

where a_{NMR} and a_{MICP} are, respectively, the amplitudes of the (incremental) NMR T_2 and MICP distributions (Figures 1 and 2). An equal sampling density for both distributions, which is required to compute $C(\rho_e)$ by Equation 4, was obtained by resampling a cubic spline fit to each MICP curve at the same frequency (10 points per decade) as the NMR T_2 distribution.

As noted by Kleinberg and others[3], this matching scheme is appropriate when the shapes of the two distributions being matched are similar to each other. Figure 1 shows this condition is well satisfied for all but one (sample 6) of the high-pressure MICP samples, implying a consistent pore body-to-throat size ratio for these samples. For the low-pressure MICP samples (Figure 2), there is a gross similarity between the shapes of the NMR T_2 and MICP distributions but the correspondence is not nearly as good as for the high-pressure samples (Figure 1). Also, a correction had to be applied to the low-pressure MICP data sets for incomplete filling of the pore space by mercury. The magnitude of the correction required was taken to be the difference between resaturation pore volume from routine core analysis (Table 1) and the total volume of mercury injected at the maximum injection pressure (2000 psi). This "missing" injection volume was arbitrarily assigned to an air/mercury capillary pressure of 5000 psi prior to computing ρ_e. These problems, and the typically lower accuracy and precision of injection volume measured with low-pressure MICP apparatus, highlight the advantages of using high-pressure MICP data for correlation with NMR relaxation time distribution.

Values for ρ_e determined by the above procedure are listed in Table 2. A noteworthy result is that the effective relaxivities for the carbonates are generally less than those for the sandstones. In fact, if sample 6 is excluded from consideration — which is reasonable

since this is the only sample that shows a poor correspondence between its NMR T_2 and MICP distributions — we find that all the limestone samples (ρ_e range = 1.0 to 3.2 μ m/sec) have smaller relaxivities than all the sandstone samples (6.4 to 25. μm/sec) and that the dolomite ρ_e values (5.4 and 4.6 μm/sec) lie between those for the limestones and sandstones. This result is consistent with previous studies[4,5] which have shown that carbonates generally have smaller surface relaxivities than sandstones.

We also note in passing that, unlike one previous study[6], our results show no significant difference between the relaxivities of clean sandstones (range = 6.4 to 23. μm/sec, average = 14. μm/sec) and shaly sandstones (range = 7.9 to 25. μm/sec, average = 16. μm/sec). In this regard, it is perhaps significant that the porosities measured by NMR are the same (within experimental error) as the routine core analysis porosities (Table 1). Evidently, the clay-bound water which presumably exists in the shaly sand samples relaxes slowly enough to be detected with the echo spacing and SNR used in our NMR measurements.

RELATIVE PERMEABILITY, FRACTIONAL FLOW, AND T_2 CUTOFFS

As noted earlier, existing NMR log interpretation models use the *irreducible* fluid volume BVI from the NMR as an estimate for the volume of *immobile* water in the formation. Standard reservoir engineering practice for estimating water-cut makes use of fractional flow which expresses the relative flow-rate of one fluid in the presence of one or more additional fluids[7]. For example, in a two-fluid phase system, the fractional flow of the wetting phase F_w is defined as

$$F_w = Q_w/(Q_w+Q_{nw}) \qquad (5)$$

where Q is a volume flow rate and the subscripts w and nw denote the wetting and non-wetting fluids, respectively.

Fractional flow is a function fluid viscosity μ and relative permeability K_r. For a two-phase system, the fractional flow equation is

$$F_w = 1/(1+(K_{rnw}/K_{rw})(\mu_w/\mu_{nw})). \qquad (6)$$

Water-cut is negligible, i.e., water is considered effectively immobile, when F_w drops below some (operationally defined) threshold value. The value of S_w is known as the "critical" water saturation which is distinct from the "irreducible" water saturation S_{wi}, e.g., as identified from a capillary pressure curve.

Standing[8] shows how to compute relative permeability from capillary pressure data. The capillary pressure curve for a rock sample and its NMR T_2 distribution measured at S_w = 100% both represent the pore size distribution. These considerations suggests the following simple procedure for computing F_w from NMR data:

1. Convert the incremental T_2 distribution into a cumulative T_2 distribution and normalize the amplitudes by the NMR porosity to obtain a curve of T_2 vs. saturation S_w. That is, convert the T_2 distribution into a "pseudo-capillary pressure curve".

2. Compute relative permeabilities from the following pair of Standings' equations[8],

$$K_{rw} = \left(S_w^*\right)^2 \times \frac{\int_0^{S_w^*} \frac{dS_w^*}{P_c^2}}{\int_0^1 \frac{dS_w^*}{P_c^2}} \quad (7) \qquad K_{rnw} = \left(1 - S_w^*\right)^2 \times \frac{\int_{S_w^*}^1 \frac{dS_w^*}{P_c^2}}{\int_0^1 \frac{dS_w^*}{P_c^2}} \quad (8)$$

where $S_w^* = (S_w - S_{wi})/(1 - S_{wi})$. T_2 can substituted directly for 1/Pc since $T_2 \propto 1/Pc$ (Equations 2 and 3). The above equations are for drainage but similar equations are available for K_r during imbibition if required. For simplicity in this preliminary application, we assume that $S_w^* = S_w$ (i.e., $S_{wi} = 0$).

3. Substitute K_{rw} and K_{rnw} computed from Equations 7 and 8 into Equation 6 to compute the fractional flow F_w as a function of S_w for a particular viscosity ratio μ_w/μ_{nw}.

For the purposes of illustration, we take the critical water saturation to be the value of S_w at which F_w=0.01, i.e., at a wetting phase flow rate equal to 1% of the total flow rate. This, in turn, defines a cutoff value of T_2 that distinguishes mobile vs. immobile fluid. Notice that, because F_w is defined in terms of the ratios of integrals of the T_2 distributions, the cutoff value of T_2 will be independent of the relaxivity ρ_e. This is not true for the standard fixed Pc cutoff models.

Table 2 shows values of S_w and equivalent air-brine Pc corresponding to the Fw=0.01 cutoff. Results are shown for two different viscosity ratios corresponding to a gas-water system (μ_w/μ_{nw}=10) and a light oil-water system (μ_w/μ_{nw}=1). T_2 at F_w=0.01 and the "typical" (i.e., fixed) T_2 cutoff for sandstones of 33 msec[9] are plotted as vertical lines with the T_2 distribution for each sample in Figures 1 and 2. T_2 at F_w=0.01 varies over about two orders of magnitude, from a few msec to several hundred msec (Table 2). Changing the viscosity ratio from 10 to 1 effects only a modest reduction in the cutoff T_2. The cutoff T_2 correlates with rock type as defined by lithology and, especially, by the well of origin. The huge range of cutoff T_2 values, which is at first startling, is a consequence of the fact that K_r and, hence, F_w depends only the *shape* of the T_2 distribution and not on its absolute position. This contrasts with the standard T_2 cutoff definitions for which the shape of the distribution is less important than its position (in T_2 time).

The P_c and S_w values at F_w=0.01 are plotted as points on the MICP curves for the carbonates and sandstone samples in Figures 3 and 4, respectively. These points span a wide range of capillary pressures and are typically located near the point of maximum curvature on the capillary pressure curve. A horizontal line corresponding to a constant capillary pressure cutoff of 50 psi (equivalent air-brine Pc) is shown for reference. Using a fixed F_w criterion usually (but not always) gives a higher estimate of immobile S_w than does the fixed Pc definition. Figure 5 shows that the agreement between critical S_w from

NMR and MICP is generally very good since the shapes of the two distribution types are very similar (except for sample 6, as already noted).

In summary, the fixed F_w model introduced here tends to predict higher values of immobile S_w and, hence, is more optimistic than the standard (fixed) Pc models. The behavior of the fixed F_w model is complex and, from an applications standpoint, has some obvious drawbacks. First, the model can succeed only if the relaxation time distribution corresponds closely to the rock pore size distribution. This poses potential problems for log interpretation in partially oil-saturated rock or in oil-wet formations. Also, successful application of the present model may require NMR data having a high SNR because noise artificially broadens peaks in the relaxation time distribution and F_w is sensitive to the *width* of the distribution. Obtaining data of the requisite SNR might require very low logging speeds.

T_2 AND PERMEABILITY

Our goal here was to test an NMR-derived analog of a parameter introduced by Swanson[10] for estimating absolute permeability. The sample suite used in this study provides a good test of the method since, as shown in Figure 6, porosity is a very poor estimator of permeability. The Swanson parameter is defined as the maximum value of the ratio BVNW/Pc where BVNW is the bulk volume of the non-wetting phase. Physically, this parameter is interpreted as representing the portion of the pore size distribution that controls fluid flow. Figure 7 illustrates the procedure for obtaining the Swanson parameter from the MICP curve for a limestone sample (#12). Figure 8 shows that max(BVNW/Pc) from MICP is an excellent permeability estimator for all the samples used in this study.

The NMR analog of Swanson's' parameter is obtained by simply converting the T_2 distribution into a pseudo-capillary pressure curve, as described in step 1 of the procedure outline above for computing fractional flow. Based on the correspondence between Pc and T_2 (Equations 2 and 3), the NMR analog of Swanson's parameter occurs at the maximum value of the product $BVNW \cdot T_2$. Figure 9 shows a cross plot of this NMR-based parameter and core permeability. Instead of a single trend, three parallel trends are observed, each of which corresponds to a different rock type. Notice that the relative positions of the trend lines are ordered by the relaxivities for the different rock types.

Figure 10 shows that, by including the factor ρ_e in the analog Swanson parameter, the three separate trends in Figure 9 can be "collapsed" into a single trend. The scatter of the data points about this trend is comparable to that obtained from MICP (Figure 8). Again, this result is expected from the good correspondence between NMR T_2 and the MICP distributions (Figures 1 and 2). These relationships are intriguing since they suggest a new method for determining relaxivity using NMR and permeability data.

CONCLUSIONS

Transverse relaxation time (T_2) distributions and mercury injection capillary pressure (MICP) distributions for the rock samples used in this study are highly correlated implying

consistent pore body-to-throat ratios for the majority of the samples. The effective relaxivity ρ_e determined by matching NMR T_2 and MICP data vary by rock type. Our results are consistent with those of prior studies which show that carbonate rocks generally have lower relaxivities than sandstones.

We have illustrated a new method for computing fractional flow F_w from T_2 distributions using standard reservoir engineering methods. The method leads to an alternative definition of cutoff T_2 that distinguishes mobile vs. immobile fluid. The T_2 cutoff corresponding to a fixed value of F_w (we used 1%) depends only on the shape of the T_2 and is independent of the surface relaxivity. In general, the present model predicts higher values of immobile water volume than the standard FFI/BVI models that use as fixed T_2 cutoff near 30 msec.

For the samples used in this study, which show essentially no correlation between porosity and permeability, an NMR-based analog of the Swanson parameter normalized by the effective relaxivity ρ_e is an excellent predictor of the permeability.

ACKNOWLEDGMENT

We thank the companies who contributed the samples and the mercury injection data used in this study and are especially grateful to Jim Klein, Ray Sorenson, Don Hartman, and Jack Horkowitz for their help in obtaining these materials.

REFERENCES

1. Kenyon, W.E., "Nuclear Magnetic Resonance as a Petrophysical Measurement", *Nucl. Geophys., 6*, 153-171 (1992).
2. Prammer, M.G., "NMR Pore Size Distributions and Permeability at the Well Site", SPE 69th Annual Technical Conference and Exhibition Proceedings, Paper SPE 28368 (1994).
3. Kleinberg, R. L., Farooqui, S. A., Horsfield, M. A., "T1/T2 Ratio and Frequency Dependence of NMR Relaxation in Porous Sedimentary Rocks", *J. Colloid Interface Sci., 158*, 195-198 (1993).
4. Timur, A., "Nuclear Magnetic Resonance Study of Carbonates Rocks", *The Log Analyst, 13*, 3-11 (1972).
5. Chang, D., Vinegar, H. V., Morriss C. E., Straley, C., "Effective Porosity, Producible Fluid and Permeability in Carbonates from NMR Logging", SPWLA 35th Annual Logging Symposium Transactions, Paper A (1994).
6. Howard, J. J., Kenyon, W. E., Straley, C., "Proton Magnetic Resonance and Pore Size Variations in Reservoir Sandstones", SPE 65th Annual Technical Conference and Exhibition Proceedings, Paper SPE 20600 (1990).
7. Craig, F.F. Jr., The Reservoir Engineering Aspects of Waterflooding, Society of Petroleum Engineers of AIME, New York, pp. 29-44 (1993).
8. Standing, M.B., *Notes on Relative Permeability Relationships*, Division of Petroleum Engineering and Applied Geophysics, The Norwegian Institute of Technology, University of Trondheim (1974).
9. Morriss, C.E., MacInnis, Freedman, R., Smaardyk J., Straley C., Kenyon, W.E., Vinegar, H.J., and Tutunjian, P.N., "Field Test of an Experimental Pulsed Nuclear Magnetism Tool", SPWLA 34th Annual Logging Symposium Transactions, Paper GGG (1993).
10. Swanson, A Simple Correlation Between Permeabilities and Mercury Capillary Pressure, *J. Petrol. Tech.*, 2498-2504 (1981).

Table 1: Basic Properties

Well Number	Sample Number	Core Porosity p.u.	Core Permeability md	Grain Density g/cm^3	NMR Porosity p.u.	Mercury Injection Type	Rock Type
1	1	23.0	0.503	2.70	23.6	Low Pres.	Shaly Sand
	2	23.1	0.245	2.70	22.1	Low Pres.	Shaly Sand
	3	26.9	117.	2.71	26.8	Low Pres.	Shaly Sand
	4	26.8	18.1	2.71	26.7	Low Pres.	Shaly Sand
	5	24.8	113.	2.71	25.2	Low Pres.	Shaly Sand
2	6	11.2	0.078	2.71	11.6	High Pres.	Limestone
	7	14.6	1.33	2.69	14.5	High Pres.	Limestone
	8	12.5	0.252	2.69	12.4	High Pres.	Limestone
3	9	10.5	12.3	2.70	10.5	High Pres.	Limestone
	10	6.4	0.287	2.70	7.4	High Pres.	Limestone
	11	7.8	1.58	2.70	7.9	High Pres.	Limestone
	12	14.9	41.4	2.71	14.6	High Pres.	Limestone
4	13	9.7	2.15	2.65	10.2	High Pres.	Clean Sand
	14	20.5	4449.	2.64	20.6	High Pres.	Clean Sand
5	15	16.7	1030.	2.64	16.4	High Pres.	Clean Sand
6	16	15.8	7.14	2.83	15.7	High Pres.	Dolomite
	17	19.2	2.54	2.85	18.1	High Pres.	Dolomite

Table 2: Comparisons of Relaxation Time Data to Mercury Injection Data

	Relaxation Time Data						Mercury Injection Data		
	effective relaxivity	μ_w/μ_{nw} = 10		μ_w/μ_{nw} = 1			μ_w/μ_{nw} = 10		
Sample #	ρ_e μm/sec	T2 @ Fw=.01 ms	Sw @ Fw=.01 %	T2 @ Fw=.01 ms	Sw @ Fw=.01 %	max BVNW·T2 p.u. ms	Pc air/brine @ F_w=.01 psi	Sw @ Fw=.01 %	max BVNW/P_c p.u./psi
1	9.98	8.83	73.9	3.69	60.7	60.2	98.2	72.6	0.018
2	7.92	7.74	68.0	4.08	52.7	62.7	110.	75.3	0.012
3	25.1	34.4	65.8	15.5	55.5	492.	6.52	58.5	0.362
4	15.8	21.0	59.7	13.4	44.2	326.	11.5	63.0	0.167
5	19.9	35.3	66.6	17.0	58.0	441.	7.08	62.9	0.287
6	12.6	57.8	78.8	31.6	69.2	198.	125.	52.9	0.009
7	3.16	88.6	58.6	57.9	43.9	672.	26.0	59.2	0.046
8	1.26	102.	69.6	57.2	56.8	502.	43.5	65.3	0.020
9	3.16	419.	49.5	307.	36.2	2791.	6.53	51.8	0.132
10	0.996	328.	60.3	212.	45.8	1203.	23.5	66.9	0.016
11	1.99	400.	60.8	243.	47.2	1619.	12.6	65.7	0.038
12	2.51	715.	41.4	583.	27.8	7872.	4.47	48.0	0.305
13	6.42	57.2	55.3	38.1	41.6	454.	16.7	54.1	0.061
14	23.0	348.	45.0	278.	30.6	4802.	1.25	42.9	1.91
15	11.1	332.	49.3	236.	35.5	3310.	1.92	39.9	0.980
16	5.34	87.3	51.6	64.1	37.9	785.	19.6	49.0	0.090
17	4.58	61.0	58.1	43.6	44.6	524.	38.0	54.8	0.051

max(BVNW/Pc) = *Swanson parameter from mercury injection data.*
max(BVNW·T2) = *NMR analog of Swanson parameter from relaxation time distribution.*
Fw = *Fractional flow*

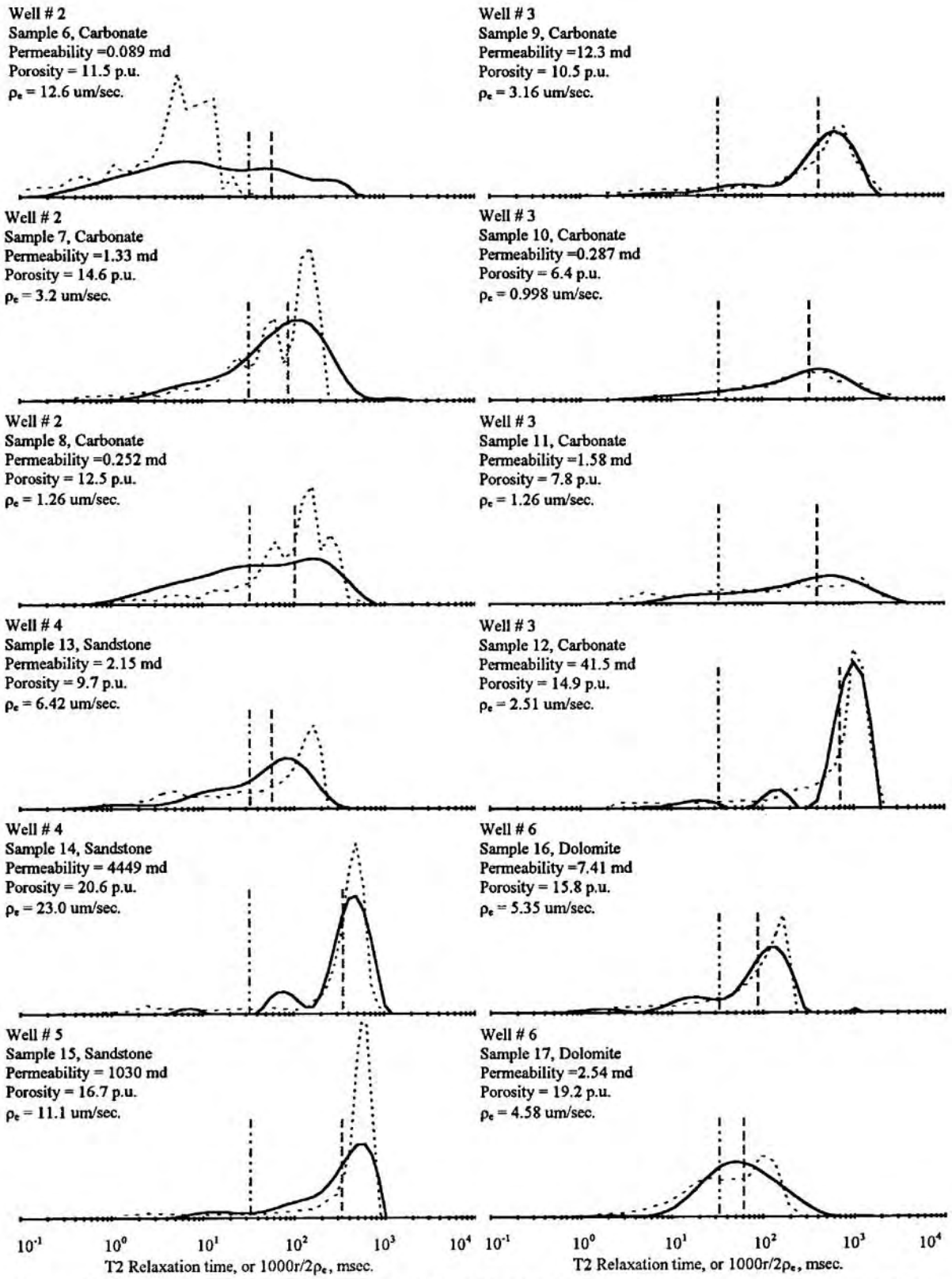

Figure 1: Incremental T2 (solid) is compared to mercury injection capillary pressure pore throat radius (r, short dashed). T2 @ Fw = .01 (long dash) was computed from the T2 distribution for μ_w/μ_{nw} = 10. A standard T2 cutoff value of 33 ms (long dash-dot-dot) is displayed for comparison.

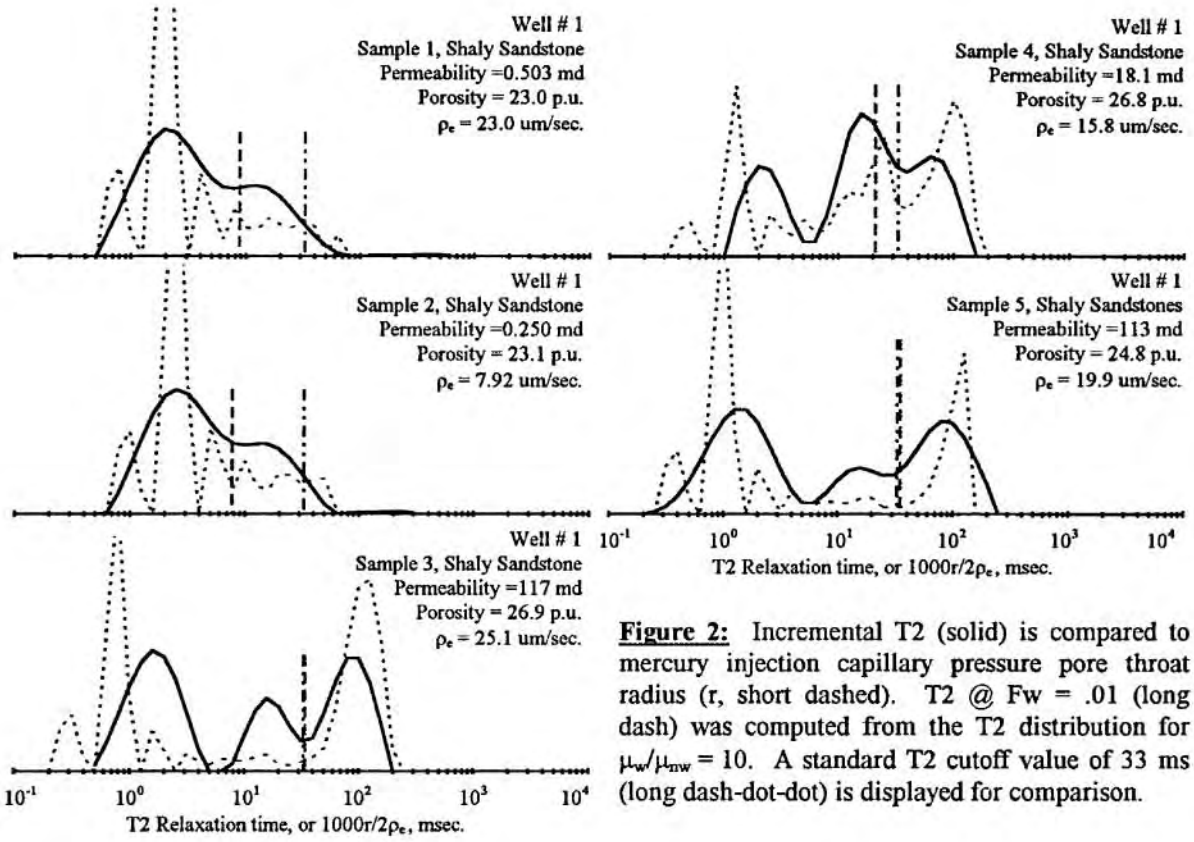

Figure 2: Incremental T2 (solid) is compared to mercury injection capillary pressure pore throat radius (r, short dashed). T2 @ Fw = .01 (long dash) was computed from the T2 distribution for μ_w/μ_{nw} = 10. A standard T2 cutoff value of 33 ms (long dash-dot-dot) is displayed for comparison.

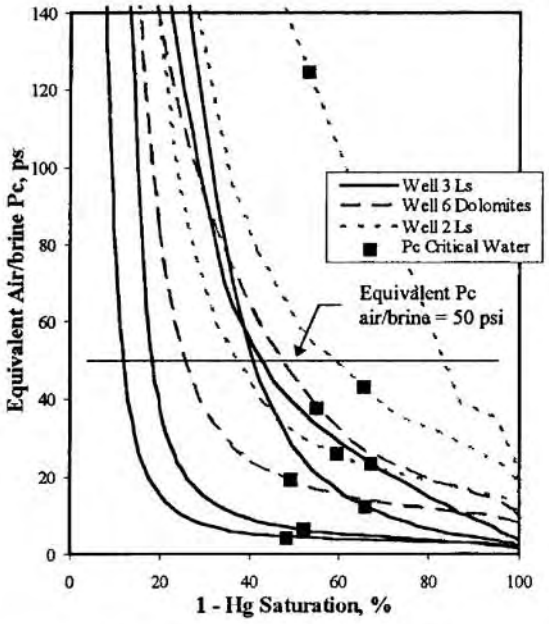

Figure 3: Pc curves for carbonate samples. Mercury injection pressure has been converted to an equivalent Pc for an air/brine system. Pc and Sw @ Fw = .01 for μ_w/μ_{nw} = 10 is plotted as a point on the Pc curve for each sample.

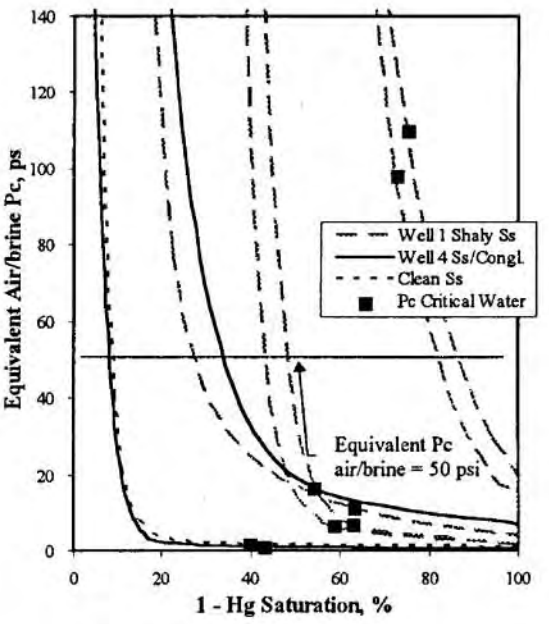

Figure 4: Pc curves for sandstone samples. Mercury injection pressure has been converted to an equivalent Pc for an air/brine system. Pc and Sw @ Fw = .01 for μ_w/μ_{nw} = 10 is plotted as a point on the Pc curve for each sample.

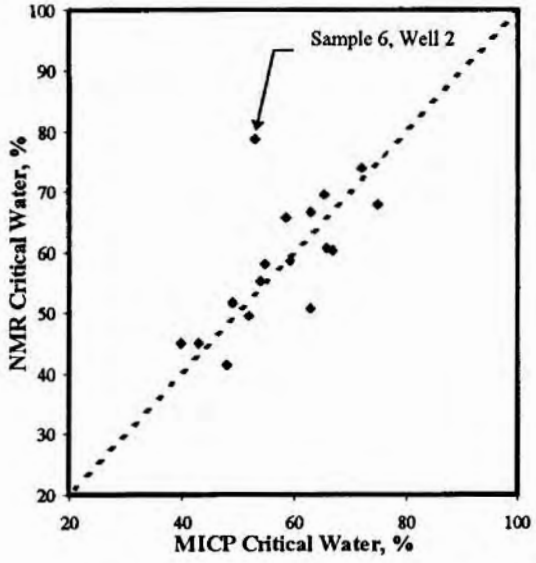

Figure 5: Comparison of critical water saturation (Fw = .01) independently determined using NMR and mercury injection capillary pressure (MICP) for $\mu_w/\mu_{nw} = 10$.

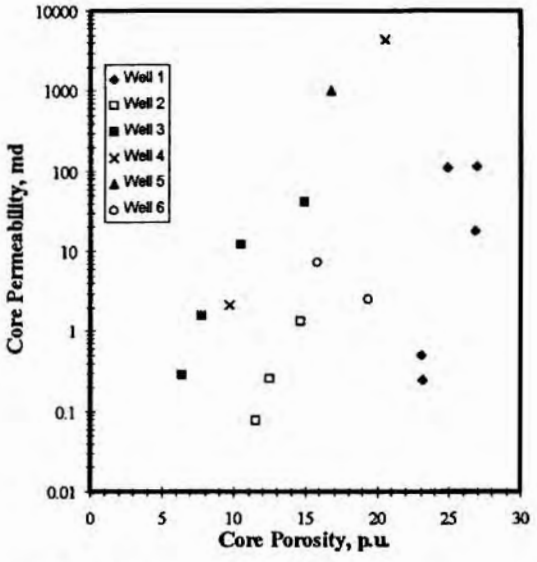

Figure 6: Core analysis permeability and porosity cross plot for all samples represented in study.

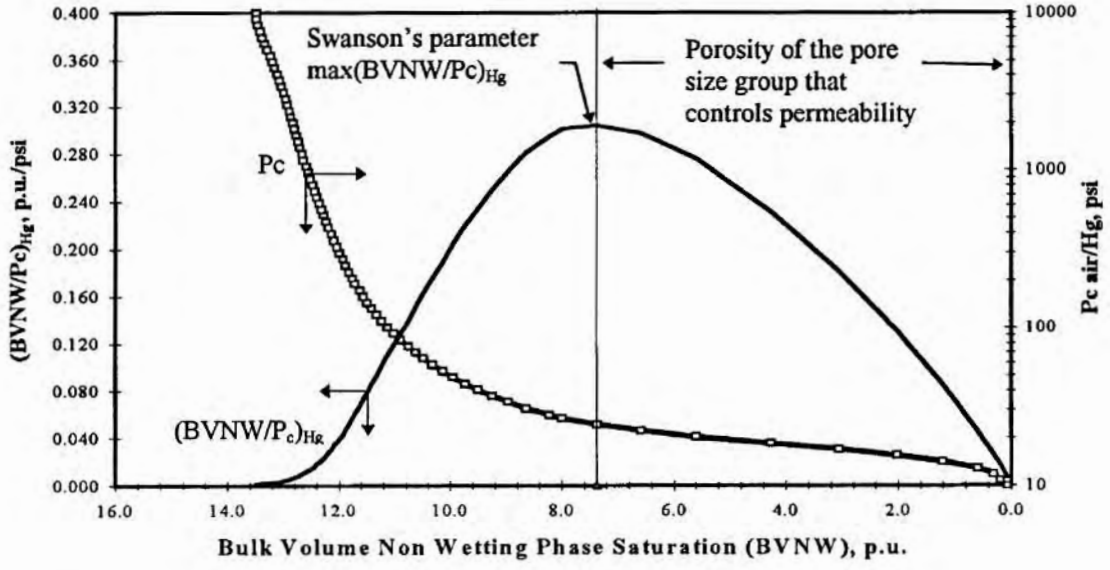

Figure 7: Method for obtaining the Swanson parameter from a mercury injection capillary pressure curve (solid line with squares). Injection volume is expressed as a percentage of bulk volume (BVNW). Swanson's parameter is defined as the maximum value of the ratio of BVNW/Pc.

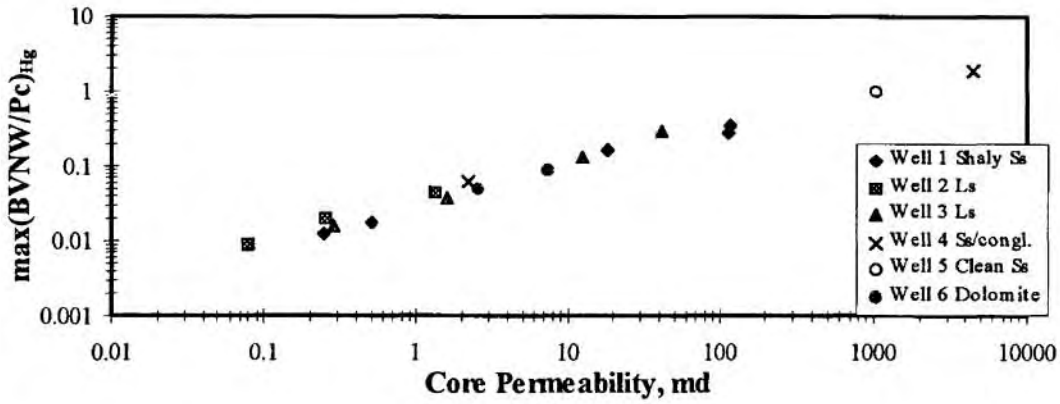

Figure 8: Cross plot of core permeability vs. Swanson's parameter from mercuy injection showing an excellent correlation.

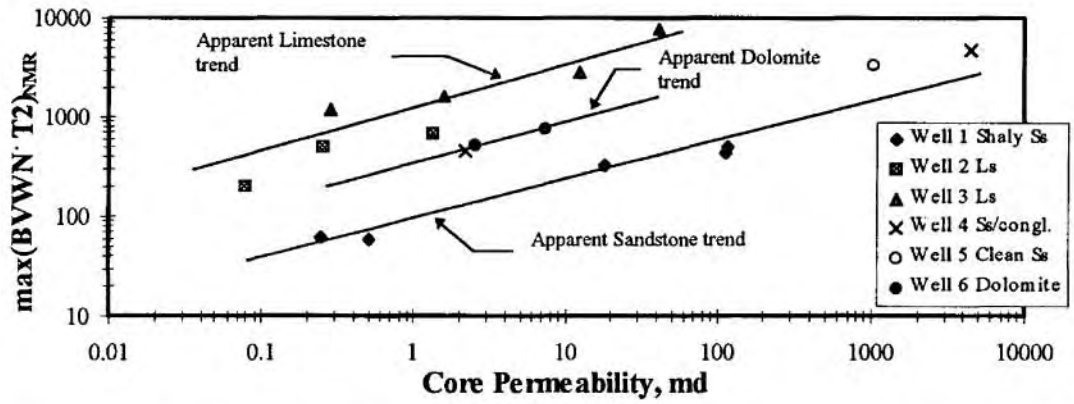

Figure 9: Cross plot of core permeability vs. NMR analog of Swanson's parameter, $\max(BVNW \cdot T2)_{NMR}$, showing distinct trends for different rock types.

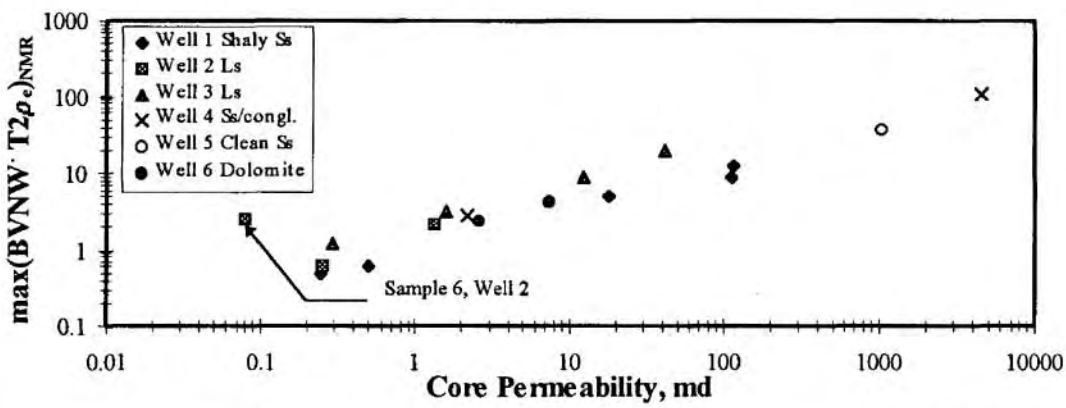

Figure 10: Cross plot of permeability vs. NMR analog of Swanson's parameter multiplied by the effective relaxivity ρ_e. Trend matches Figure 8 demonstrating that $\max(BVNW \cdot T2\rho_e)_{NMR}$, like Swanson's parameter, is an excellent predictor of permeability. Departure of sample #6 from the trend is attributed to a poor match between MICP and NMR distributions.